Effect of surrounding soil on elasto-plastic dynamic response of underground structures to near-fault ground motions

Kemal Hacıefendioğlu
Assoc. Prof. Dr.Ondokuz Mayis University , Samsun, Turkey, hckemal@omu.edu.tr

Gökhan Saraçoğlu
Research Asistant, Ondokuz Mayis University, Turkey, gokhan.saracoglu@omu.edu.tr

KEYWORDS: Tunnels, soil effects, nonlinear behavior.

ABSTRACT: Soil characteristics are important for the earthquake behavior of structures, especially underground structures such as tunnels. This study explains that the soil effects on the displacement and stress components of dynamic behavior for underground tunnels. A reinforced concrete underground tunnel, which are modeled for three different soil types and the results show the effects of soil parameters on dynamic behavior. Duzce Earthquake acceleration record is used as near fault ground motion. The nonlinear behavior of the tunnel-soil interaction systems is idealized as elasto-plastic using the Drucker-Prager model. Displacement and stress values are given by graphical represent at the end of paper.

1 INTRODUCTION

It is usually accepted that underground structures suffer less from earthquakes than superstructures. However, recent earthquakes as in Kobe Japan earthquake, Chi-Chi Taiwan earthquake (Chen et al. 2002) and Kocaeli Turkey earthquake (Hashash et al. 2001) caused extensive failure in tunnels. Underground structure damages were also observed in different earthquakes, such as 1976 Tangshan earthquake in China (Wang 1985) and the Loma Prieta earthquake in USA. It is obvious that the safety of mountain tunnels in seismically active areas is still an important issue to tunnel engineers.

2 NUMERICAL SOLUTION OF DYNAMIC EQUILIBRIUM EQUATION

The matrix equation of motion with nonlinear stiffness under earthquake excitation for multi-degree of freedom system can be written as;

$$M\ddot{U}(t) + C\dot{U}(t) + K(U)U(t) = -Ma(t) \quad (1)$$

where M, C and K are the mass, damping and stiffness matrix, respectively. $\ddot{U}, \dot{U}$ and U are the vectors of the acceleration, velocity and displacement, respectively. Solution of this equation is carried out in time domain using the Newmark β Method.

The damping matrix is proportional the mass and stiffness matrices:

$$[C] = \alpha[M] + \beta[K] \qquad \alpha = \frac{2\omega_i\omega_j(\zeta_i\omega_j - \zeta_j\omega_i)}{\omega_j^2 - \omega_i^2}, \qquad \beta = \frac{2(\zeta_j\omega_j - \zeta_i\omega_i)}{\omega_j^2 - \omega_i^2} \tag{2}$$

where ω_i, ω_j are the first and second modes, and ζ_i, ζ_j are two values of damping for the first and second normal modes of vibration, respectively. The final expression of equation of motion with nonlinear behavior obtained by substituting the required parameters and equations into Eq. (1) leads the following relationships:

$$\tilde{q}_{k+1} = \tilde{F}_N^{(n)}\tilde{q}_k + \tilde{H}_N^{(nEQ)}a_{k+1} - \tilde{H}_N^{(nEQ)}a_k \tag{3}$$

Where $\tilde{q}_{k+1} = \{U_k \quad \dot{U}_k \quad \ddot{U}_k\}^T$. The $\tilde{F}_N^{(n)}$ and $\tilde{H}_N^{(nEQ)}$ matrices are functions of the time, and these matrices are computed at each time step. The superscript (n) denotes nonlinear time history analysis.

$\tilde{F}_N^{(n)}$ and $\tilde{H}_N^{(nEQ)}$ matrices are

$$\tilde{F}_N^{(n)} = \begin{bmatrix} I & (\Delta t)I - \alpha(\Delta t)^3 B^{-1}K_s \\ \mathbf{0} & I - \delta(\Delta t)^2 B^{-1}K_s \\ \mathbf{0} & -(\Delta t)B^{-1}K_s \end{bmatrix}$$

$$\begin{bmatrix} \frac{1}{2}(\Delta t)^2 I - \alpha(\Delta t)^3 B^{-1}C - \frac{1}{2}\alpha(\Delta t)^4 B^{-1}K_s \\ (\Delta t)I - \delta(\Delta t)^2 B^{-1}C - \frac{1}{2}\delta(\Delta t)^3 B^{-1}K_s \\ I - (\Delta t)B^{-1}C - \frac{1}{2}(\Delta t)^2 B^{-1}K_s \end{bmatrix} \tag{4}$$

$$\tilde{H}_N^{(nEQ)} = -\begin{bmatrix} \alpha(\Delta t)^2 B^{-1}M \\ \delta(\Delta t)B^{-1}M \\ B^{-1}M \end{bmatrix} \tag{5}$$

where I is a unit matrix, and α, δ presents numerical solution method constants, respectively. Eq(4) and Eq.(5) matrices require the inversion of the B matrix at each time step and it follows that

$$B = M + \delta(\Delta t)C + \alpha(\Delta t)^2 K_s \tag{6}$$

3 ELASTO PLASTIC MATERIAL MODEL

The tangent stiffness matrix for the elasto-plastic behavior of dynamic system can be written as:

$$K^{e}_{(n)} = \int_V B^{(e)T} D^{(e)}_{ep} B^{(e)} dV \tag{7}$$

where $B^{(e)}$ and $D^{(e)}_{ep}$ present the strain-displacement and elasto-plastic rigidity matrices for each element, respectively. $D^{(e)}_{ep}$ matrix depends on the yield surface defined by Drucker-Prager failure criterion function (Drucker & Prager 1952). The failure criterion function for solid elements can be expressed as follows:

$$f(I_1, \sqrt{J_2}) = \sqrt{J_2} + \frac{sin\emptyset}{\sqrt{3}(3 - sin\emptyset)} I_1 - \frac{6ccos\emptyset}{\sqrt{3}(3 - sin\emptyset)} = 0 \tag{8}$$

where I_1 is the first principal invariant, and J_2 is the second stress deviator. In Eq(8) (*c*) and ($\emptyset$) are the cohesion and angle of internal friction of the material, respectively.
For the elasto-plastic materials, the general incremental stress-strain relations are written as;

$$d\sigma_{ij} = D^{ep}_{ijkl} d\varepsilon_{kl} = 2G\tilde{\delta}_{ik}\tilde{\delta}_{jl} + \left(K - \frac{2}{3}G\right)\tilde{\delta}_{ij}\tilde{\delta}_{kl} - \frac{1}{\breve{H}}\breve{H}_{ij}\breve{H}_{kl} \tag{9}$$

$$,\breve{H}$$

For Drucker-Prager model, and $\breve{H}_{ij}$ are given follows:

$$\breve{H} = 9K\left(\frac{sin\emptyset}{\sqrt{3}(3 - sin\emptyset)}\right)^2 + G \tag{10}$$

and

$$\breve{H}_{ij} = 3K\left(\frac{sin\emptyset}{\sqrt{3}(3 - sin\emptyset)}\right)\tilde{\delta}_{ij} + \frac{G}{\sqrt{J_2}} s_{ij} \tag{11}$$

where K and G are bulk and shear modulus of material, respectively. In Eq.(11) s_{ij} presents deviatoric stress tensor (Chen & Mizuno 1990).

According to classical theory of plasticity, the incremental plastic strains are proportional to the derivative of the yield function with respect to the incremental stresses (Chen & Han, 1988):

$$d\varepsilon_{ij}^{p} = d\lambda \frac{df}{d\sigma_{ij}} \tag{12}$$

where $d\lambda$ is the plastic multiplier. $d\varepsilon_{ij}^{p}$ is the incremental plastic strain tensor.

4 NONLINEAR EARTHQUAKE BEHAVIOUR OF THE TUNNEL MODEL

This study involves finite element dynamic analysis of a reinforced concrete tunnel and the different soil effects on it. Geometric properties and dimensions are represented in Figure 1. Tunnel was modeled with three different soil types in order to compare the earthquake behavior in various cases.

Soil properties used in the analyses are summarized in Table 1. It is obvious that, elasticity, Poisson's ratio and mass density are directly related with the dynamic behavior. The tunnel has one tube and it includes reinforced concrete and shotcrete concrete. The radius of tunnel is 6.25 m. However, the thickness of the concrete is variable. It has a thickness of 0.4m at the top of the tunnel, but the thickness increases through the base and it has 0.67m thickness at the road level. Finite element model was prepared by using ANSYS (2010) software for three different soil types. 2497 PLANE42 elements are used in the finite element method for the tunnel (Sevim 2011) As boundary conditions, the viscous boundary supports were used for soil characterization.

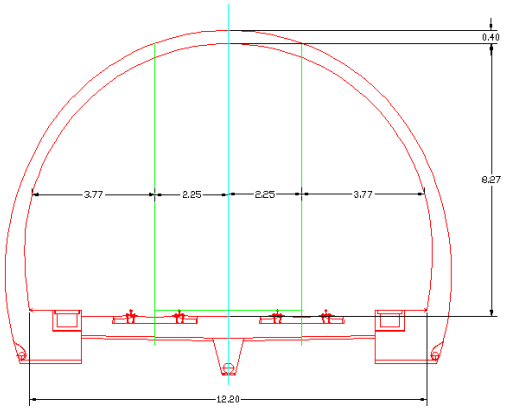

Figure1: Geometric properties of tunnel

Table1 Soil properties for each model

Soil Types	Modulus of Elasticity (N/m^2)	Poison Ratio	Mass Density (kg/m^3)	Cohession (N/m^2)	Internal Friction
1	7,62E+10	0,26	2678,90	3,1E+6	40
2	1,20E+10	0,14	2548,20	2,7E+6	38
3	1,77E+09	0,45	2069,32	3,25E+6	32

5 APPLICATION

Duzce Earthquake (1999) acceleration record was applied to tunnel models for the nonlinear transient analyses (figure 3). This earthquake occured in North Anatolian Fault which is the most active seismic region on Turkey. The Drucker-Prager model is selected for the nonlinear analyses of a reinforced concrete tunnel and soil types and its smooth failure surface provides very definite

analytical and computational advantages (Barla 2008). The element matrices were computed using the Gauss numerical integration technique (Bathe 1996) in the analyses. The Newmark method is used in the solution of the equation of motion. Rayleigh damping coefficients assumed 5% damping ratio.Displacement and stress values are obtained and represented on the graphs for some special nodes such as A,B,C,D,E,F and G.

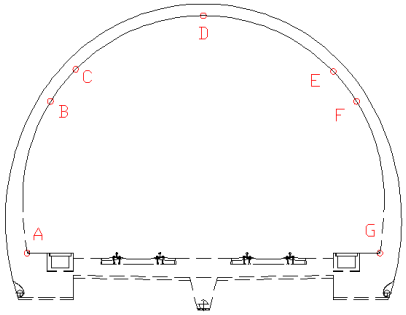

Figure 2 : Selected nodes for the time history of the displacement and stress values.

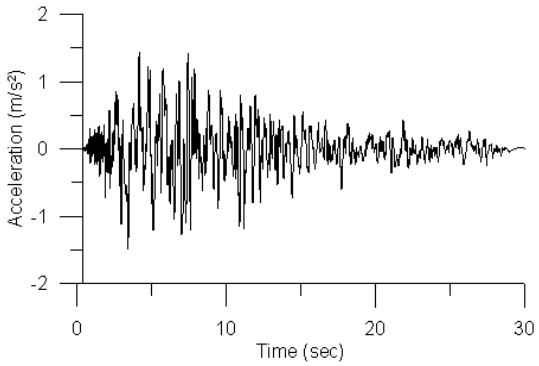

Figure 3: Acceleration Time History for Duzce Earthquake

5 DISPLACEMENTS

The maximum horizontal displacement values through distance of the tunnel are presented in Figure 3. This figure represents the maximum displacement values on selected nodes (A,B,C,D,E,F,G) for each tunnel model. The third soil types has the lowest modulus of elasticity, for this reason displacement reached the maximum level on the third tunnel section. Maximum displacement values are occured on the top of the tunnel for the three soil types. Peak values are 0,000104995 m for the first soil type, 0,000587527 m for second soil type and 0,00516802 for third soil type. These values are within the allowable limits for earthquake phenomena.

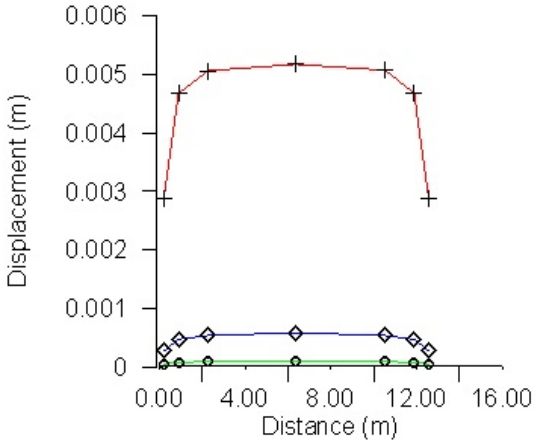

Figure 4: Displacements through section of the tunnel

6 PRINCIPAL STRESSES

Figure 4 shows the variation of maximum principal stresses on the tunnel section. As it can be seen from the figure, the maximum stresses are small at the top of the tunnel, even so they are high at the bases. The first soil type has the lowest modulus of elasticity, for this reason stress reached the maximum level on the third tunnel section. The stresses obtained for the section have a symmetrical distribution. Figure 5 shows the variation of minimum principal stresses on the tunnel section. Minimum stresses have a symmetrical distribution like the maximum principal stresses, as a consequence of indiscrete material properties and geometrical shape.

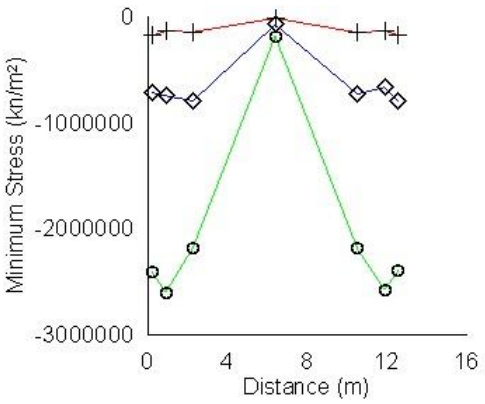

Figure 5 Maximum Stresses

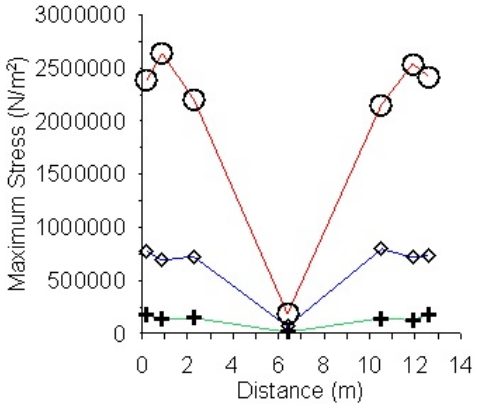

Figure 6 Minimum Stresses

The maximum and minimum principal stress contours for the soil types are presented in Figure 6(a-c) and Figure 7(a-c). As it is seen from the figures, the maximum and minimum principal stresses occur at the base of the tunnel.

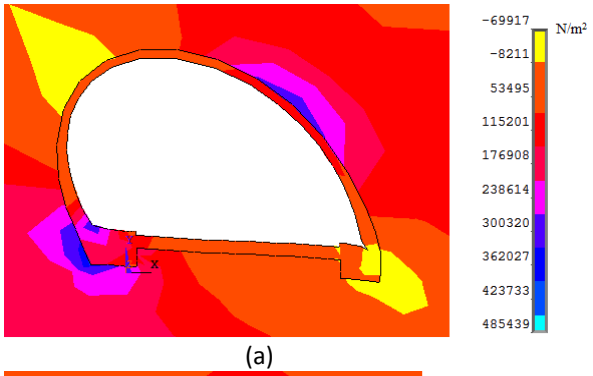

(a)

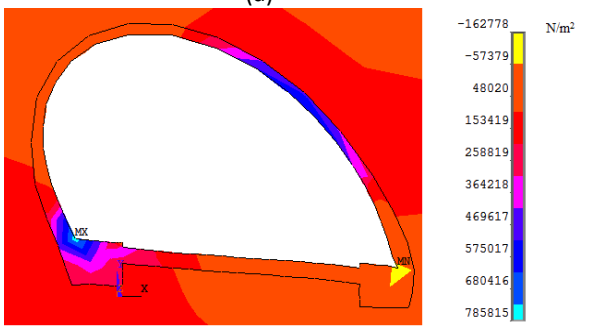

(b)

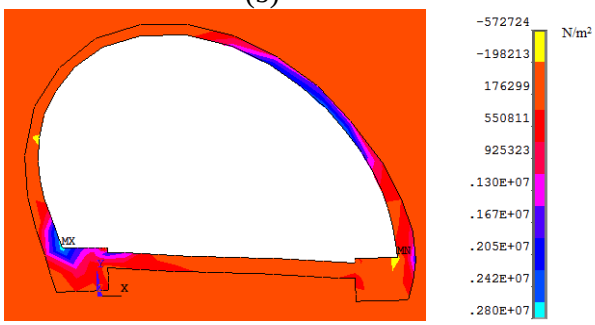

(c)

Figure 7 Maximum stress contours (a) first, (b) second and (c) third soil types

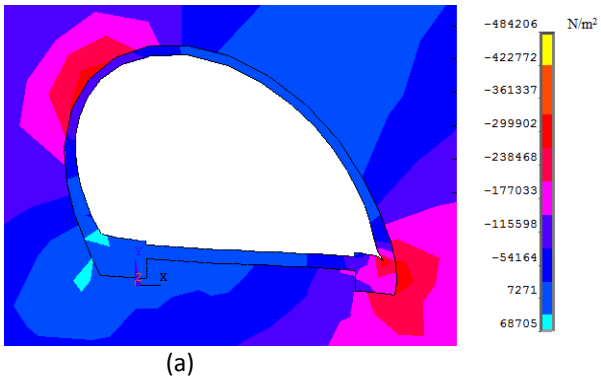

(a)

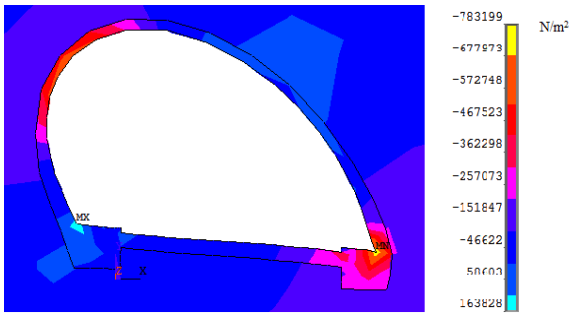

(b)

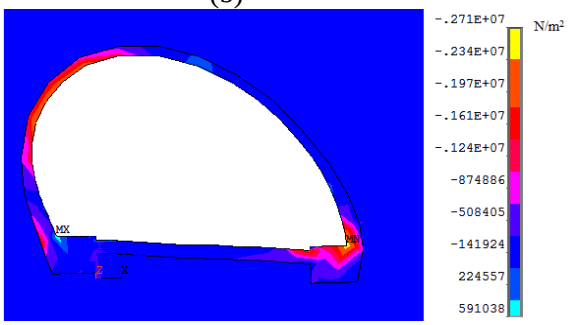

(c)

Figure 8 Minimum stress contours a) first, (b) second and (c) third soil types

7 CONCLUSIONS

This paper considers the surrounding soil effects on the nonlinear earthquake behavior of underground tunnels. The finite element model is prepared for each soil type and the analyses realized with ANSYS software. Düzce Earthquake acceleration record was used as near fault ground motion. Results showed that the modulus of elasticity, Poison's ratio and mass density play crucial role for the displacement and stress values during earthquake actions. Stress values are mostly important on the base of tunnel structures when displacements are critical for the top of tunnel section.

REFERENCES

Barla, M. (2008). Numerical simulation of the swelling behaviour around tunnels based on special triaxial tests.Tunnelling and Underground Space Technology Incorporating Trenchless Technology Research, 23(5), 508-521. doi:10.1016/j.tust.2007.09.002

Bathe, K. (1996). Finite element procedures. Englewood Cliffs, N.J: Prentice Hall.

Chen, W. W., Chen, Y., Shih, B., Hung, J., & Hwang, H. H. (2002). Seismic response of natural gas and water pipelines in the ji-ji earthquake. Soil Dynamics and Earthquake Engineering, 22(9), 1209-1214. doi:10.1016/S0267-7261(02)00149-5

Chen, W., & Han, D. J. (1988). Plasticity for structural engineers. New York: Springer-Verlag

Chen, W., & Mizuno, E. (1990). Nonlinear analysis in soil mechanics: Theory and implementation. Amsterdam: Elsevier.

Drucker, D.C., Prager, W. (1952). Soil mechanics and plastic analysis on limit design, Quart. J. Appl. Math. 10, 157-165.

Hashash, Y. M. A., Hook, J. J., Schmidt, B., & I-Chiang Yao, J. (2001). Seismic design and analysis of underground structures. Tunnelling and Underground Space Technology Incorporating Trenchless Technology Research, 16(4), 247-293. doi:10.1016/S0886-7798(01)00051

Sevim, B. (2011). Nonlinear earthquake behaviour of highway tunnels. NATURAL HAZARDS AND EARTH SYSTEM SCIENCES, 11(10), 2755-2763. doi:10.5194/nhess-11-2755-2011

Jing-Ming, W. (1985). The distribution of earthquake damage to underground facilities during the 1976 tang-shan earthquake.Earthquake Spectra, 1(4), 741. doi:10.1193/1.15852